Journal of the Meteorological Society of Japan, Vol. 90, No. 4, pp. 553−573, 2012
DOI: 10.2151/jmsj.2012-408

Circulation and Eddy Kinetic Energy Budget Analyses on the Evolution of a Northeast China Cold Vortex (NCCV) in May 2010

Shenming FU

International Center for Climate and Environment Sciences, Institute of Atmospheric Physics, Chinese Academy of Sciences, Beijing, China

and

Jianhua SUN

Laboratory of Cloud-Precipitation Physics and Severe Storms, Institute of Atmospheric Physics, Chinese Academy of Sciences, Beijing, China

(Manuscript received 23 May 2011, in final form 28 May 2012)

Abstract

A typical Northeast China cold vortex (NCCV) that lasted for approximately 51 hours (from 0000 UTC 18 May to 0300 UTC 20 May, 2010) and produced several heavy rainfall events over Northeast China was successfully simulated using the Weather Research and Forecasting Model (WRF). Based on this successful simulation, the NCCV was analyzed in detail. Synoptic analyses revealed that the NCCV developed downward from the top and finally stretched to a maximum vertical extension of 900–200 hPa. The NCCV was colder than its surroundings in the middle-lower troposphere, whereas in the upper troposphere, it was warmer than its surroundings. There were significant warm and cold advections for the duration of the NCCV, favoring the enhancement of available potential energy (APE) and conducive to sustaining the vortex. The results of the quasi-Lagrange-form eddy flux circulation (EFC) and eddy kinetic energy (EKE) budget analyses indicate that different factors dominated the NCCV in various stages of its evolution. As for the EFC budget, the interactions between the NCCV and background circulations were more important than the interactions between the vortex and other synoptic systems; in contrast, for the EKE budget, the interactions between the NCCV and other synoptic perturbations were more important. The pattern of environmental circulations was very important to the NCCV because the vortex intensified as it moved from areas of low vorticity or EKE to areas with higher values. The baroclinic energy conversion was much greater than the barotropic energy conversion during the life cycle of the NCCV, implying that the NCCV was a typical baroclinic cyclone. Moreover, during the decaying stage, the attenuation of the NCCV appeared to be closely related to the frequency dispersion processes of the baroclinic Rossby wave.

1. Introduction

Cut-off lows (COL), defined as closed cyclonic vortices in the middle-upper troposphere, are usually smaller than a mature extratropical cyclone and normally persist for a few days, although they can last for as long as three weeks in some cases (Price and Vaughan 1992; Trigo et al. 1999). A COL is cut off from a pre-existing cold trough at the middle or upper troposphere, ultimately forming an isolated cyclonic vortex (Palmen and Newton 1969). The troposphere associated with a COL is generally highly unstable, and severe convective events may occur when favorable surface conditions arise (Palmen and Newton

Corresponding author: Shenming Fu, Institute of Atmospheric Physics, Chinese Academy of Sciences, Huayanli #40, Chaoyang District, Beijing 100029, China.
E-mail: fusm@mail.iap.ac.cn

1969; Tao et al. 1980; Price and Vaughan 1992; Zhao and Sun 2007).

The COLs over Northeast China are mainly located at 36–60°N, 115–145°E and have been defined as NCCV by Chinese meteorologists (Zheng et al. 1992). However, compared with the typical COLs over North America and Europe, the cutting-off process of NCCVs is less obvious; moreover, the intensity of NCCVs are usually weaker than those of typical COLs over North America and Europe, and thus their lifetimes are shorter (Tao et al. 1980; Zhao and Sun 2007). The NCCVs exert great influences on the climate and weather of the Northeast China, Korea, East Russia and Japan due to their long persistence and high frequency (Tao 1980; Zhou 1991; Zheng et al. 1992; Huang et al. 1997). Statistical studies have indicated that NCCVs occur throughout the year and markedly impact summer weather (Sun et al. 1994; Zhao and Sun 2007). NCCVs can produce low temperatures and cold damage, heavy rainfall, flooding and intense convective activities (Tao 1980; Zhao et al. 1980; Bai 1997; Zhao and Sun 2007; Qi et al. 2007; Shou and Xu 2007; Zhang and Li 2009).

Because of their importance, many studies have focused on NCCVs. The methodologies of these works can be divided into three main areas: The first aspect entails climatological and statistical studies of NCCVs (Zhou 1991; Zheng et al. 1992; Liu et al. 2002; He et al. 2006); the second examines the background environmental conditions affecting the occurrence and development of NCCVs (Zhu 1997; Liu et al. 2002; He et al. 2006); and the third aspect focuses on the mesoscale systems producing convective weather associated with the NCCVs (Sun et al. 2000; Wang et al. 2007;Qiao et al. 2007; Zhao and Sun 2007; Zhang et al. 2008). Several studies have employed synoptic analysis and climatological correlation analysis methods to elucidate the formation and evolution mechanisms of NCCVs. For example, Huang et al. (1997) noted that an upper-level jet (ULJ) was favorable for the formation of an NCCV. Liu et al. (2002) found that both the subtropical high over the west Pacific and the blocking high in East Asia notably influence the evolution of the NCCV. Moreover, Mao and Qv (1997) calculated the energy budget of an NCCV and found that baroclinic energy conversion was very important for the maintenance of the vortex; however, their calculation was based on a low-resolution data set that only includes 10 vertical levels at a horizontal resolution of 5º × 5º.

The detailed evolution of the NCCV and the interactions between the NCCV and other systems are unclear due to a lack of observation and effective diagnostic tools. Therefore, the purposes of this study are as follows: (1) to understand the mechanisms of the formation and evolution of the NCCV with effective diagnostic tools and (2) to examine the interactions between the NCCV and other systems in detail.

During the spring of 2010, NCCVs are active over Northeast China and precipitate several heavy rainfall events. An NCCV that lasted for approximately 51 hours (from 0000 UTC 18 May to 0300 UTC 20 May, 2010) with a maximum 6-h precipitation of 23 mm was selected for further analysis in this study because this vortex presents a typical case according to its statistical characteristics (i.e., its horizontal scale, moving track, range of influence, life span and the intensity of associated precipitation) of the NCCV (Zheng et al. 1992; Liu et al. 2002; He et al. 2006). Moreover, we were able to collect sufficient data for detailed studies, e.g., both surface observations and soundings.

The eddy flux circulation (EFC) budget equation (Davis and Galarneau 2009) and the eddy kinetic energy (EKE) budget equation (Ding and Liu 1985; Fu et al. 2009) are utilized to analyze the evolution and the energy characteristics of the NCCV, respectively. Moreover, the EFC and EKE budgets could validate each other, resulting in a more thorough understanding of the evolution of the NCCV. The newly developed EFC budget equation is a very useful tool for diagnosing the evolution of vortices and the interactions among vortices and other synoptic systems and environmental circulations. Davis and Galarneau (2009) investigated the evolution of two developing mesoscale convective vortices using the EFC budget equation and successfully analyzed the dominant factors during different developmental stages of the vortices. The EKE budget equation has been successfully used to investigate the formation and evolution of different types of cyclones (Ding and Liu 1985; Orlanski and Katzfey 1991; Liu and Liang 1993; Fu et al. 2009). The data and diagnostic methods utilized in this study are introduced in Section 2. The synoptic conditions of the NCCV are described in Section 3. The results of the EFC and EKE budgets for different stages of the NCCV are discussed in Section 4. Finally, the summary and conclusions are presented in Section 5.

2. Numerical simulation configuration, data and methodology

2.1. Numerical simulation configuration and data

The weather research and forecasting model (WRF) is a next-generation mesoscale forecast model (Michalakes et al. 2004). The advanced research WRF (ARW) version 3.3 was employed in this study. Final analy-

sis data (at a resolution of 1º × 1º) from the National Centers for Environmental Prediction (NCEP/FNL) were used for the initial and boundary conditions in the simulation. Moreover, 12-h soundings and 3-h surface observations from the China Meteorological Administration (CMA) were used to improve the first guess through the objective analysis method. The WRF model was run with two domains of two-way nesting together with surface and observational nudging in the outer domain. The reciprocal value of the damping time constant was set at 0.0003, which is an appropriate value for our simulation. The simulation was initialized at 1200 UTC 17 May, 2010, 12 h before the initial formation of the NCCV, and integrated for 72 h to include the entire lifetime of the cyclone. The horizontal grid spacings of the outer and inner domains were 30 km and 10 km, with 23×190 and 511 × 421 grid points, respectively. The centers of the outer and inner domains were set at (41ºN, 105ºE) and (44.255ºN, 112.225ºE), respectively, as shown in Fig. 1, there are 35 eta levels, with the top at 50 hPa. Model instantaneous outputs were saved every 3 h for the outer domain and every 1 h for the inner domain. The outputs from the WRF were interpolated to 37 pressure levels: 1000-100 hPa (interval: 25 hPa). The simulation results of the inner domain were used for calculations and analysis during the entire lifetime of the cyclone. The Kain-Fritsch (Kain and Fritsch 1990; Kain 2004) cumulus parameterizations and YSU Planetary Boundary Layer schemes (Hong et al. 2006) were used in the simulations.

2.2. *The EFC budget equation*

The circulation budget equation proposed by Davis and Galarneau (2009) is as follows:

$$\frac{\partial C}{\partial t} = \underbrace{-\bar{\eta}\tilde{\delta}A}_{\text{Stretching}} \underbrace{-\oint \eta' \vec{V}_h{}' \cdot \vec{n} dl}_{\text{Eddy Flux}} + \underbrace{\oint \omega(\vec{k}\times\frac{\partial \vec{V}_h}{\partial p})\cdot\vec{n}dl}_{\text{Tilting}} + \underbrace{\oint (\vec{k}\times\vec{F}_h)\cdot\vec{n}dl}_{\text{Friction}} \quad (1)$$

where the term associated with background circulation, i.e., $\oint \eta' \overline{\vec{V}_h} \cdot \vec{n} dl$, was neglected by the authors because the effects of background circulation were much smaller than the other terms in their study. However, in the present study, the term associated with background circulation was retained because it was important for the development of the NCCV. A term including friction and sub-grid processes (*RES*) was also defined, and then Eq. (1) was rewritten in a quasi-Lagrangian form[1]:

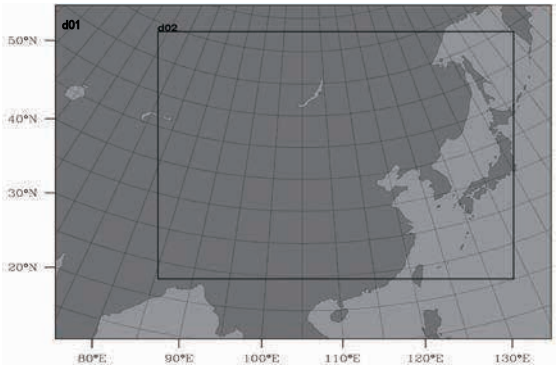

Fig. 1. The illustration of the double-nested grid system, where d01 represents the outer domain and d02 stands for the inner domain.

$$\frac{\delta C}{\delta t} = \underbrace{\overline{M}_h \cdot \nabla_h C}_{\text{Motion-caused Flux}} \underbrace{-\bar{\eta}\tilde{\delta}A}_{\text{Stretching}} \underbrace{-\oint \eta' \overline{\vec{V}_h} \cdot \vec{n} dl}_{\text{Background Flux}} \underbrace{-\oint \eta' \vec{V}_h{}' \cdot \vec{n} dl}_{\text{Eddy Flux}} + \underbrace{\oint \omega(\vec{k}\times\frac{\partial \vec{V}_h}{\partial p})\cdot\vec{n}dl}_{\text{Tilting}} + \underbrace{RES}_{\text{Residual term}} \quad (2)$$

where $\delta C/\delta t$ is the quasi-Lagrangian variation of the circulation following the system, $\overline{M}_h$ is the horizontal velocity of the system, $\nabla_h = \partial/\partial x\vec{i} + \partial/\partial y\vec{j}$, $\vec{V}_h = u\vec{i} + v\vec{j}$ is the horizontal wind field, $C = \oint \vec{V}_h \cdot d\vec{l}$ is the circulation along the system boundary, η is the absolute vorticity, $\tilde{\delta}$ is the system-area average divergence, A is the area of the target system (in this study, the KA of the NCCV is used), ω is the vertical velocity in pressure coordinates, $\vec{n}$ is the unit vector normal to the boundary line of the system, $\vec{k}$ is the unit vector in the vertical direction, p is the pressure, and $\vec{F}_h$ is the horizontal friction. Overbars indicate the average values around the perimeter of the target system, and primes denote perturbations from the average values. Davis and Galarneau (2009) explained the tilting term [$\oint \omega(\vec{k}\times\partial\vec{V}_h/\partial p)\cdot\vec{n}dl$] with a vortex line view; however, they did not explain why the horizontal vorticity[2] in the tilting term contains only the

[1]The quasi-Lagrangian form equation is derived by an approximation as follows: $\delta A/\delta t = \partial A/\partial t + \overline{M}\cdot\nabla_h A$, where A is the focused meteorological quantity, $\delta A/\delta t$ is the quasi-Lagrangian variation of A, and $\overline{M}$ is the horizontal velocity of the system.

[2]In full, the horizontal vorticity vector is $(\partial w/\partial y - \partial v/\partial z)\vec{i} + (\partial u/\partial z - \partial w/\partial x)\vec{j}$.

vertical shear component of the horizontal wind. In this study, we developed a concise alternative description for the tilting term in terms of circulation and answered the above question reasonably.

Bringing the hydrostatic equation ($\partial p/\partial z = -\rho g$) into the tilting term $\oint \omega(\vec{k}\times\partial\vec{V}_h/\partial p)\cdot\vec{n}dl$, and defining the simplified form of the horizontal vorticity vector as $\vec{\omega}_{xy} = (-\partial v/\partial z\vec{i} + \partial u/\partial z\vec{j})$, we deduce that $\oint \omega(\vec{k}\times\partial\vec{V}_h/\partial p)\cdot\vec{n}dl = \oint w\vec{\omega}_{xy}\cdot\vec{n}dl$, where w is the vertical velocity in the system coordinates (x, y, z, t). For an example, circulation was assumed along a polygon L (Fig. 2), and the section of line AB was studied. The whirling around the horizontal vorticity vector (the ellipses in Fig. 2) modifies the circulation along the polygon L. When the tilting term is not equal to 0, then $\vec{\omega}_{xy}$ cannot be normal to $\vec{n}$ (i.e., $\vec{\omega}_{xy}\cdot\vec{n} \neq 0$, $\vec{\omega}_{xy}$ cannot parallel the boundary line), and $w \neq 0$. The horizontal vorticity vector can decomposed into a component along the boundary line ($\vec{\omega}_2$) and a component normal to the boundary ($\vec{\omega}_1$; Fig. 2). The whirling around $\vec{\omega}_2$ thus has no effect on the velocity along the section of line AB because they are orthogonal. As a result, the tilting term is zero when the horizontal vorticity parallels the boundary line, which means that the whirling around the horizontal vorticity vector cannot modify the circulation along the polygon L. The whirling around $\vec{\omega}_1$ is parallel to the boundary line, and the whirling modifies the velocity along the boundary line significantly when there is obvious vertical motion[3]. The complete form of the horizontal vorticity vector is $(\partial w/\partial y - \partial v/\partial z)\vec{i} + (\partial u/\partial z - \partial w/\partial x)\vec{j}$, and it is obvious that the horizontal vorticity in the x direction is composed of two terms: $\partial w/\partial y$ and $\partial v/\partial z$. The term $\partial w/\partial y$ is caused by the horizontal shear in the vertical motion; however, because the vertical motion w is normal to the horizontal wind, the vertical motion has no impact on the horizontal velocity along the boundary line of the polygon L, which means that the circulation along the polygon L cannot be modified by the vertical velocity. Similarly, $\partial w/\partial x$ has no effect on the circulation along polygon L. Therefore, the tilting term does not include the two terms associated with the horizontal shear in the vertical motion. Based on the previous analysis, the tilting term thus reflects the effects of small whirling around the horizontal vorticity vector on the large circulation associated with the vertical vorticity. The influence of the tilting term is also verified in our case, as discussed in Sub-subsection 4.1.a.

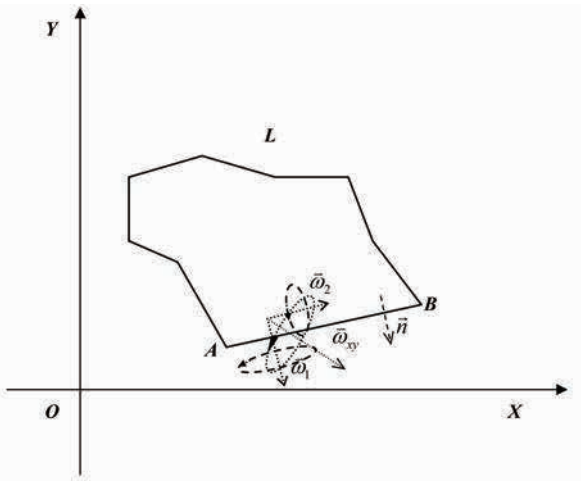

Fig. 2. The schematic of the horizontal vorticity and the tilting term where the polygon L represents the boundary line of the research area; $\vec{n}$ is the unit vector normal to the boundary line; $\vec{\omega}_{xy} = \vec{\omega}_1 + \vec{\omega}_2$ is the horizontal vorticity vector; and the ellipses stand for the whirling 6 associated with the vorticity vectors.

2.3. *The EKE budget equation*

The EKE budget equation used by Ding and Liu (1985) and Fu et al. (2009) is as follows:

$$\frac{\delta\overline{[K_E]}}{\delta t} = \underbrace{I(K_Z, K_E)}_{\text{Term 1}} + \underbrace{I(P_E, K_E)}_{\text{Term 2}} + \underbrace{F_H(K_E)}_{\text{Term 3}} + \underbrace{F_V(K_E)}_{\text{Term 4}} + \underbrace{F_C(K_E)}_{\text{Term 5}} + \underbrace{F_H(P_E)}_{\text{Term 6}} + \underbrace{F_V(P_E)}_{\text{Term 7}} + \underbrace{D(K_E)}_{\text{RES}} \quad (3)$$

where $K_Z = 1/2(\overline{[u]^2 + [v]^2})$ stands for the area-averaged zonal mean kinetic energy, $K_E = 1/2(u'^2 + v'^2)$ is the EKE per unit mass, and P_E is the geopotential perturbation per unit mass. The left-hand side of Eq. (3) is the quasi-Lagrangian of the area-averaged EKE, and the right-hand side terms of the equation are defined as

[3]Using a sufficiently small round area centered on an arbitrary point on a section of line AB, we can assume that the motions have the same linear velocity and the same radius inside this area. As a result, when there is no vertical motion, there is no effect on the velocity along the boundary line because this section of line AB passes through the center of the small area. When vertical motion occurs, the small area moves up or down, and the velocity along the boundary is modified by the linear velocity of the small round, which in turn influences the circulation along the boundary line.

Terms 1 through 7 and *RES*:

$$I(K_Z, K_E) = -\overline{[u'v']\frac{\cos\varphi}{a}\frac{\partial}{\partial\varphi}\frac{[u]}{\cos\varphi}} - \overline{[v'v']\frac{1}{a}\frac{\partial[v]}{\partial\varphi}} - \overline{[u'\omega']\frac{\partial[u]}{\partial p}} - \overline{[v'\omega']\frac{\partial[v]}{\partial p}} + \overline{[u'u'][v]\frac{\tan\varphi}{a}} \quad \text{(Term 1)}$$

represents the transition between the zonal mean kinetic energy and EKE, i.e., the barotropic energy transition.

$$I(P_E, K_E) = -\frac{R}{p}\overline{[\omega'T']} \quad \text{(Term 2)}$$

represents the transition between APE and EKE, i.e., the baroclinic energy conversion.

$$F_H(K_E) = -\left[\overline{\frac{1}{a\cos\varphi}\frac{\partial(uK_E)}{\partial\lambda}}\right] - \left[\overline{\frac{1}{a\cos\varphi}\frac{\partial(vK_E\cos\varphi)}{\partial\varphi}}\right] \quad \text{(Term 3)}$$

is the horizontal transportation of EKE by the background circulation.

$$F_V(K_E) = -\left[\overline{\frac{\partial(\omega K_E)}{\partial p}}\right] \quad \text{(Term 4)}$$

represents the vertical transportation of EKE by background circulation.

$$F_C(K_E) = \left[\overline{\frac{c_\lambda}{a\cos\varphi}\frac{\partial K_E}{\partial\lambda}}\right] + \left[\overline{\frac{c_\varphi}{a\cos\varphi}\frac{\partial(K_E\cos\varphi)}{\partial\varphi}}\right] \quad \text{(Term 5)}$$

represents the horizontal divergence of EKE caused by system movement (where $\vec{C} = C_\lambda\vec{i} + C_\varphi\vec{j}$ is the horizontal velocity vector of the system).

$$F_H(P_E) = -\left[\overline{\frac{1}{a\cos\varphi}\frac{\partial(u'\phi')}{\partial\lambda}}\right] - \left[\overline{\frac{1}{a\cos\varphi}\frac{\partial(v'\phi'\cos\varphi)}{\partial\varphi}}\right] \quad \text{(Term 6)}$$

represents the horizontal eddy flux divergence of eddy geopotential energy, namely, the horizontal transport of eddy geopotential energy by horizontal wind perturbation.

$$F_V(P_E) = -\left[\overline{\frac{\partial(\omega'\phi')}{\partial p}}\right] \quad \text{(Term 7)}$$

represents the vertical eddy flux divergence of eddy geopotential energy, namely, the vertical transport of eddy potential energy by vertical wind perturbation. The *RES* term $D(K_E) = \delta\overline{[K_E]}/\delta t - \Sigma_{i=1}^{7}$ *Termi* accounts for effects on EKE due to friction and sub-grid processes. (For convenience, the composite effects of Terms 1 through 7 are defined as *Total* = $\Sigma_{i=1}^{7}$ *Termi*.) In the above-mentioned definitions, [ ] indicates a zonal mean, which represents the background circulation; thus, the variables can be written as $p = [p] + p'$, where p' represents eddy, and $\overline{[p]}$ stands for the area-averaged variable. Here, φ is latitude, λ is longitude, a is the radius of the earth, u is the zonal wind, v is the meridional wind, R is the gas constant, and ϕ is the geopotential.

3. Simulation validation, environmental circulation and structure of the NCCV

3.1 Simulation validation

Figure 3 illustrates the simulated geopotential height and temperature fields at 500 hPa and the corresponding observations at typical stages of the NCCV. At 1200 UTC 18 May, the simulated low center of the NCCV is at 5414 m (Fig. 3c), which is 1 gpm higher than the observation (Fig. 3a). Moreover, the simulated cold area (<–20ºC) of the NCCV is larger than the observed area. However, the location of the NCCV and the major characteristics of the synoptic circulations agree well with the observations. At other typical stages (Fig. 3), the simulation also captures the main characteristics of the observations, although there are slight differences.

Figure 4 presents the simulated and observed 6-h precipitation; however, it should be noted that the observations outside China are not complete. Two precipitation centers are observed at 0600 UTC 18 May, in east Inner Mongolia and near Korea (Fig. 4a). The intensity and location of the simulated precipitation area in Inner Mongolia closely resemble the observations, whereas the simulated precipitation area near Korea is approximately 200 km away from the observed location. At other typical times (Figs. 4b–d), the locations and intensities of the simulated precipitation areas also agree well with the observations, although there are several differences between the simulated and observed precipitation centers. As described above, although there are differences between the simulation and observation, the simulation still successfully captures the major characteristics of this event, and this simulation was thus used for further studies.

3.2 Environmental circulation and structure of the NCCV

According to evolutions of the geopotential height (Fig. 3), wind field (Fig. 5), vertical stretching (Fig. 6) and EKE during the lifetime of the NCCV, four stages (i.e., the formation stage, developing stage, maintaining stage and decaying stage) and their corresponding KAs and vertical stretching are shown in Fig. 6. Typical stages, indicated by triangles in Fig. 6, were selected for simple but representative studies.

a. The formation stage of the NCCV (2100 UTC 17 May to 0000 UTC 18 May)

There was a very deep eastward-moving trough over East Asia (106–122ºE) that stretched from 900 hPa to 200 hPa with an intense low center of 997 hPa at the surface (not shown). The deep trough tilted westward with height and was followed by a temperature trough behind it, both of which indicate that the deep trough is a developing system. The 200-hPa ULJ occurred at approximately 40ºN, and the 700-hPa lower-level jet (LLJ) appeared ahead of the deep trough (not shown), favoring moisture transport for the precipitation associated with the NCCV.

At 0000 UTC 18 May, the NCCV formed with a low center of 5480 gpm, a positive vorticity center above 20×10^{-5} s^{-1} and a cold center at less than –20ºC at 500 hPa (not shown). The typical observed sounding within KA1 (Fig. 5a) shows a moisture-rich zone at approximately 700 hPa, with very low moisture above 300 hPa (Fig. 7a). The environmental conditions within KA1 were unfavorable for convective activities because the convective available potential energy (CAPE) equals 0. The wind shear between 300 hPa and 700 hPa was 10 m s^{-1}, indicating that the baroclinity was strong. The maximum wind velocity and wind shear appeared at 300 hPa, and there was an obvious inversion layer above 300 hPa.

Ascending motions were weak within the KAs but intense to the east of the NCCV (Fig. 8e), where precipitation occurred. Warm and cold advections appeared to the east and west of the NCCV (Fig. 8a), corresponding to the southerly and northerly wind centers, respectively. Within KA1, areas of negative temperature deviation dominated the levels below 250 hPa (Fig. 8a), whereas areas of positive temperature deviation dominated the levels above 250 hPa, and the vertical distribution also indicates that the atmosphere layer was unfavorable for convective activities.

b. The developing stage (0000 UTC 18 May to 1800 UTC 18 May)

The westward-tilting deep trough and the NCCV moved eastward (Fig. 5), the close low center at 500 hPa enhanced significantly (5413 gpm, Fig. 3a), and the surface low-pressure center also intensified markedly (990 hPa). Moreover, intense cold centers appeared below 700 hPa (not shown), which means the NCCV is a very deep system (Fig. 6) according to the thermal wind relation. The ULJ near 40ºN intensified significantly, especially to the east of the NCCV (not shown), and the southwesterly LLJ also enhanced which was favorable for increased precipitation (6-h precipitation greater than 23 mm was observed). The moisture was mainly transported by the southeasterly wind from the Bohai Sea, the Yellow Sea, and the Sea of Japan (not shown). The sounding shows that the layer was moist below 500 hPa but dry above 400 hPa (Fig. 7b). The environmental conditions within KA5 remained unfavorable for convective activities (CAPE=0). The wind velocity increased significantly from 925-150 hPa (Fig. 7b), and the wind shear between 300 hPa and 700 hPa intensified significantly (30 m s^{-1}), favoring baroclinic instability. Moreover, the wind direction varied slightly at different levels, which also indicates that the NCCV is a very deep system.

Ascending motions enhanced significantly within the KAs of the NCCV (Fig. 8f), although the CAPE is very small (the simulated CAPE within the KAs was less than 34 J kg^{-1}). The enhancement of the ascending motion was due to the baroclinic instability, which was closely associated with the energy conversion between the APE and kinetic energy. New northerly wind centers formed in the lower troposphere within the KAs (Fig. 8f), which caused intense cold advections, and the temperature deviation subsequently decreased significantly (Fig. 8b).

c. The Maintaining stage (1800 UTC 18 May to 1800 UTC 19 May)

The deep trough and the NCCV moved eastward slowly (Fig. 3e), whereas the temperature trough behind it moved much faster; thus, the temperature trough caught up with the deep trough, and were in almost the same phase (Fig. 3e), which indicates that the baroclinity weakened gradually. At 0000 UTC 19 May, the upright stretching of the deep trough indicates that the trough had matured (not shown). The close low center at 500 hPa reached its minimum of 5380 gpm (Fig. 3b), and the surface low center associated with the NCCV also reached its minimum of 985 hPa (not shown) and then weakened gradually. The cold center at 500 hPa weakened with time and finally disappeared at 1200 UTC 19 May (Fig. 3e).

The wind velocity decreased above 450 hPa (Fig. 7c) and increased below 450 hPa. The wind shear between 300 hPa and 700 hPa (15 m s^{-1}) decreased remarkably, which also indicates that the baroclinity weakened. The wind direction varied slightly at 900-200 hPa, which indicates that the NCCV remained very deep (Fig. 6). The middle-lower troposphere below 600 hPa was wet, whereas it was very dry above 600 hPa. The ascending motions weakened within the KAs (Fig. 8g). The northerly wind near the western boundary of the KAs intensified markedly and caused intense cold

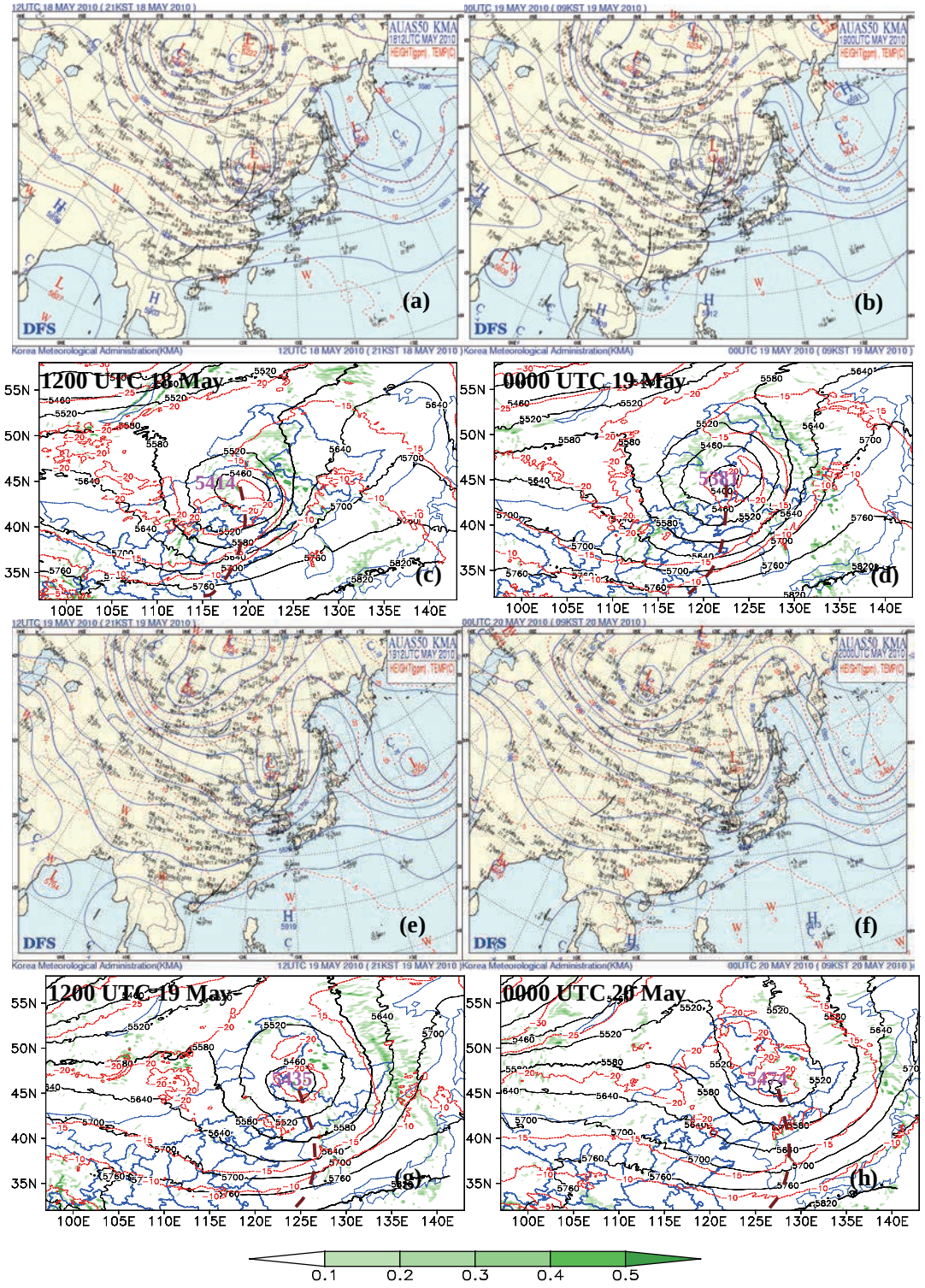

Fig. 3. Panels (a), (b), (e), and (f) are observations at 500 hPa from KMA; panels (c), (d), (g), and (h) are simulated geopotentail height (black solid; unit: m), ascending motions (shaded; unit: m s^{-1}) as well as temperature field (red dashed, unit: °C).

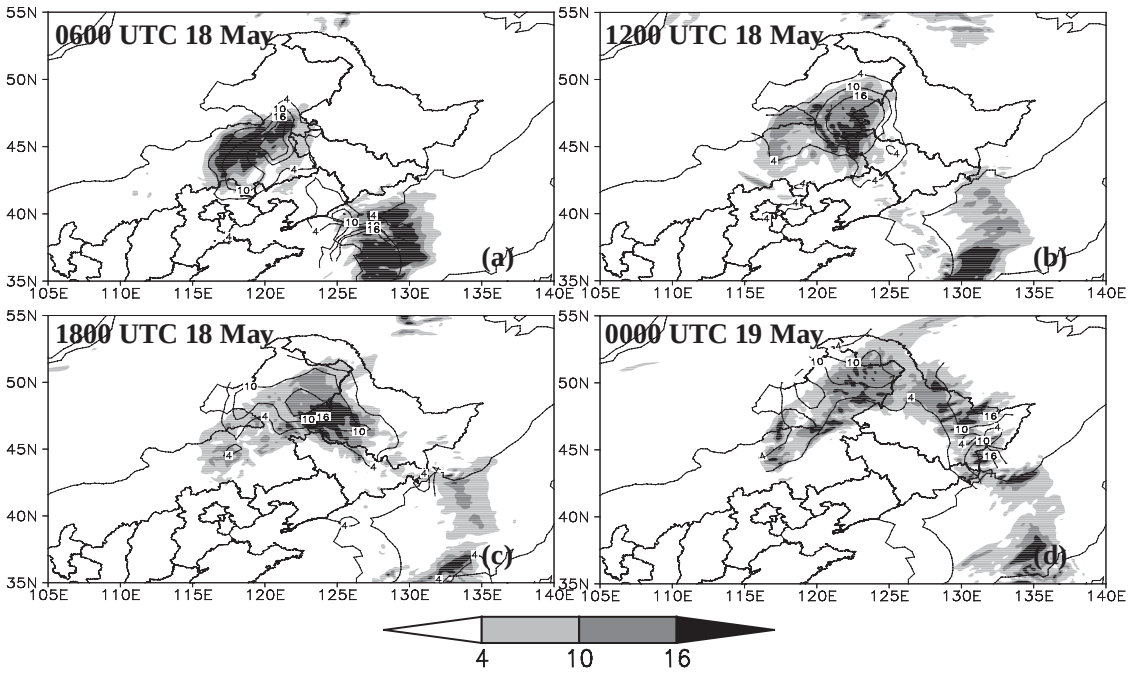

Fig. 4. Simulated 6-hour precipitation (shaded, unit: mm) and observed 6-hour precipitation (solid, unit: mm).

advections (Fig. 8c). The negative temperature deviation zones moved eastward relative to the KAs, indicating that the temperature trough moved faster than the NCCV, and thus weakened the baroclinity. Intense warm advections occurred in the cold regions in the east of the KAs, which accelerated the disappearance of the negative temperature deviations.

d. The decaying stage (1800 UTC 19 May to 0600 UTC 20 May)

The deep trough moved eastward slowly along with the temperature trough (Fig. 3f), and the trough tilted eastward slightly (not shown), which indicates the trough was weakening. The NCCV also moved eastward slowly and the KAs of the vortex shrank with time (Figs. 5h, i). The close low center at 500 hPa weakened and finally disappeared at 0000 UTC 20 May (Fig. 3f), and the surface low center dissipated at 1200 UTC 20 May. Both the ULJ and the LLJ weakened significantly (not shown), and the precipitation produced by the NCCV also weakened.

The wind velocity decreased at all levels (Fig. 7d), and the wind directions clearly varied at different levels, indicating that the NCCV had begun to shrink vertically. Wet and dry layers were located below 650 hPa and above 500 hPa, respectively, and the CAPE was zero, which was unfavorable for convective activities. The ascending motions weakened significantly and were mainly located in the east of the KAs (Fig. 8h). The weakened northerly and southerly winds associated with the NCCV resulted in remarkably decreasing cold and warm advections (Fig. 8d). The negative temperature deviation areas within the KAs also weakened, and the warm advections in the cold areas accelerated the disappearance of the cold areas. The weakening and vanishing of these cold areas suggests that the NCCV was decaying.

4. Results of the EFC and EKE budgets

4.1. The EFC budget results

Convergence zones varied significantly during the lifetime of NCCV: they were intense and located at middle-lower troposphere during the formation and developing stages (Fig. 9a) and weakened significantly during the maintaining stage finally, new convergence zones appeared in the middle-upper troposphere during the decaying stage. The divergence zones were intense during the formation and developing stages, whereas from the latter period of the maintaining stage onward, these zones weakened significantly and stretched

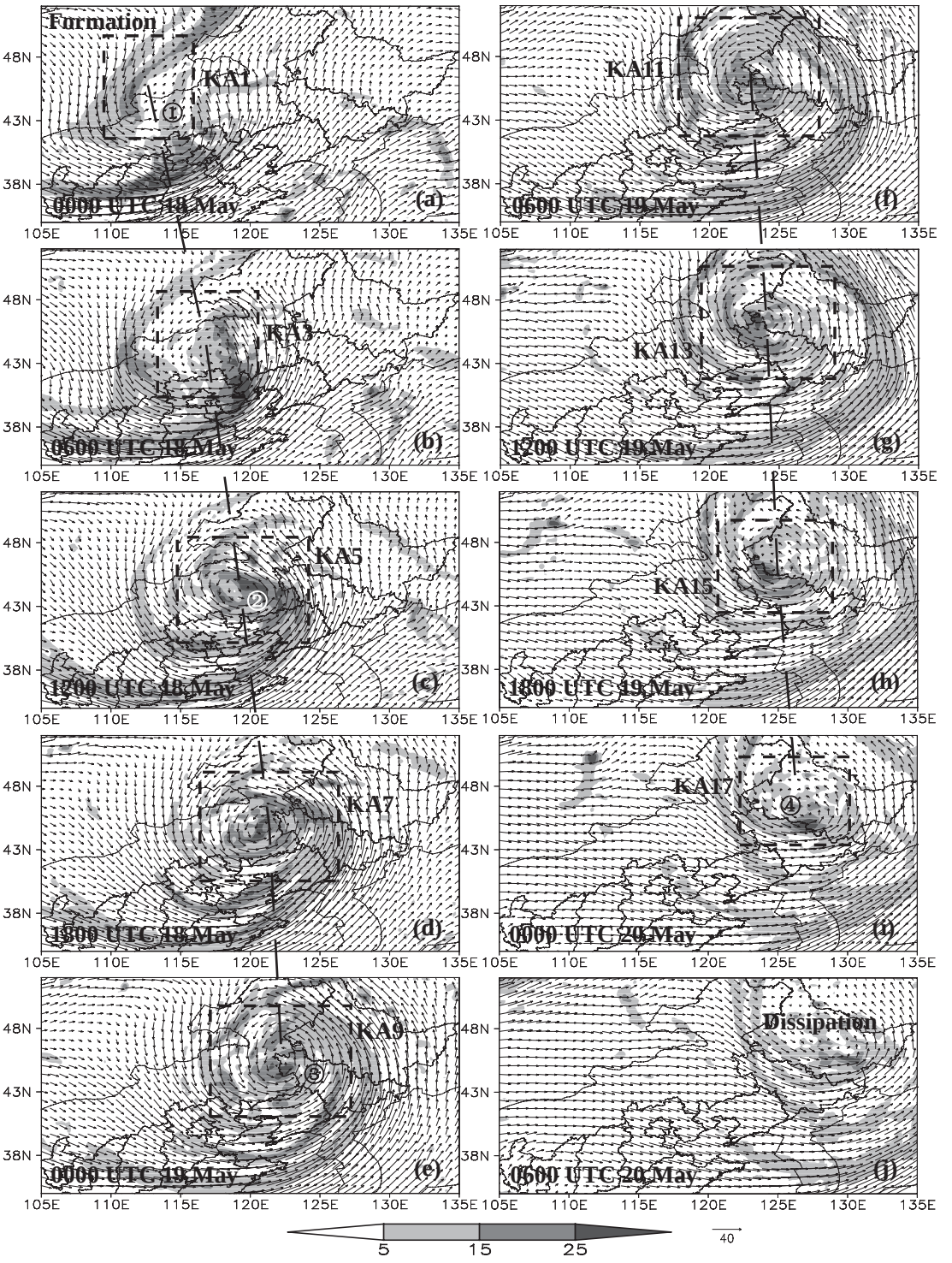

Fig. 5. The wind field (vector, unit: m s^{-1}) and vorticity (shaded, units: 10^{-5} s^{-1}) at 500 hPa, where dotted rectangles are key areas of the NCCV, dashed lines stand for the displacement of the vortex, and numbers ① − ④ stand for the location of soundings.

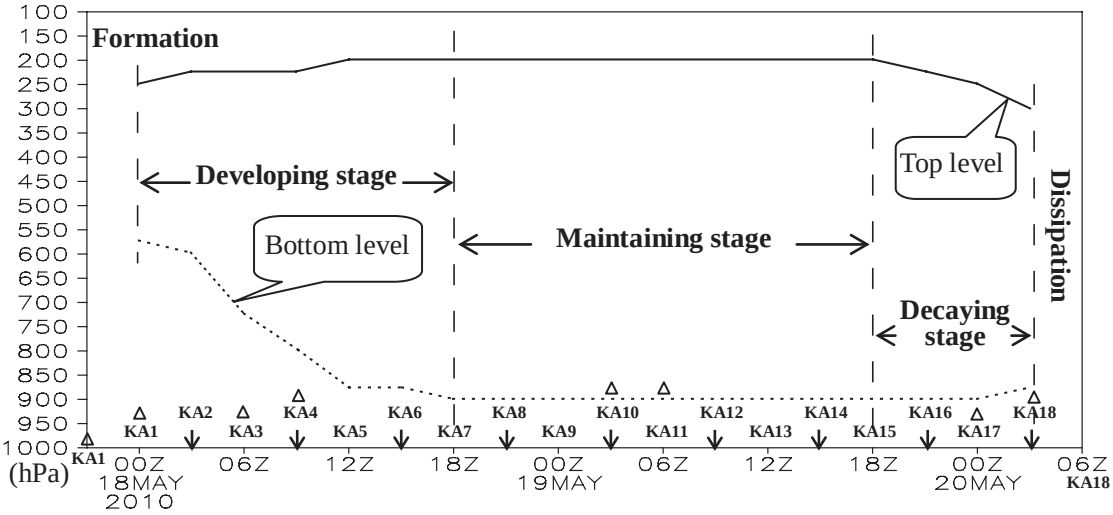

Fig. 6. The evolution, vertical stretching and key areas of the NCCV, where the triangles stand for the typical stages of the NCCV.

downward. Although the *RES* terms (representing friction and sub-grid processes) were neglected, the overall balance of the budget was generally reasonable (Fig. 9b); therefore, the budget results of EFC can be used for further research, and the evolution of the NCCV in the four typical stages is discussed in the following.

a. The formation stage of the NCCV (2100 UTC 17 May to 0000 UTC 18 May)

Before the NCCV formed, there were positive vorticity and divergence centers near 250 hPa, and a convergence center appeared at approximately 500 hPa (Fig. 9a). The stretching due to convergence and background flux were both conducive to the formation of the NCCV (Figs. 9d, e). However, when the NCCV formed, the vorticity weakened, mainly due to the eddy flux and tilting (Figs. 9a, b, f, g). The tilting term had a negative center near 300 hPa (Fig. 9g), and detailed analysis was employed to understand the tilting term in this real case. As discussed in Subsection 2.2, only $(-\partial v/\partial z)\vec{i} + (\partial u/\partial z)\vec{j}$ remains in the tilting term. Along the southern boundary of KA1, the vertical shear of zonal wind was positive (Fig. 10a); thus, the corresponding angular velocity vector pointed into KA1. The ascending motion elevated the cycling corresponding to the angular velocity and enhanced the easterly wind along the southern boundary, which in turn enhanced the clockwise circulation around the boundary line of KA1; therefore, the effect was detrimental to the cyclonic circulation. Similarly, along the western boundary of KA1, the descending angular velocity pointing to the outside of KA1 (Fig. 10a) enhanced the southerly wind along the western boundary, which in turn enhanced the clockwise circulation around the boundary line. Therefore, the distribution was also detrimental to the generation of cyclonic circulation. This process could alternatively be explained from a vortex-line viewpoint (Davis and Galarneau 2009): the ascent of the vortex-inward line (i.e., pointing into the KA) and the descent of the vortex-outward line (i.e., pointing out of the KA) produced anti-cyclonic vorticity inside the KA, weakening the cyclonic circulation of the NCCV while enhancing the cyclonic vorticity outside the KA.

b. The developing stage (0000 UTC 18 May to 1800 UTC 18 May)

During the initial period of the developing stage, the motion-caused flux, the stretching due to convergence and the eddy flux were all very favorable for the development of the NCCV (Figs. 9c, d, f); therefore, the NCCV stretched obviously downward (Fig. 6). During the latter period of the developing stage, the background flux and the stretching term due to convergence dominated the EFC budget at the upper levels of the NCCV (ULN) and the lower levels of the NCCV (LLN), respectively. To better understand the terms representing the motion-caused flux and the

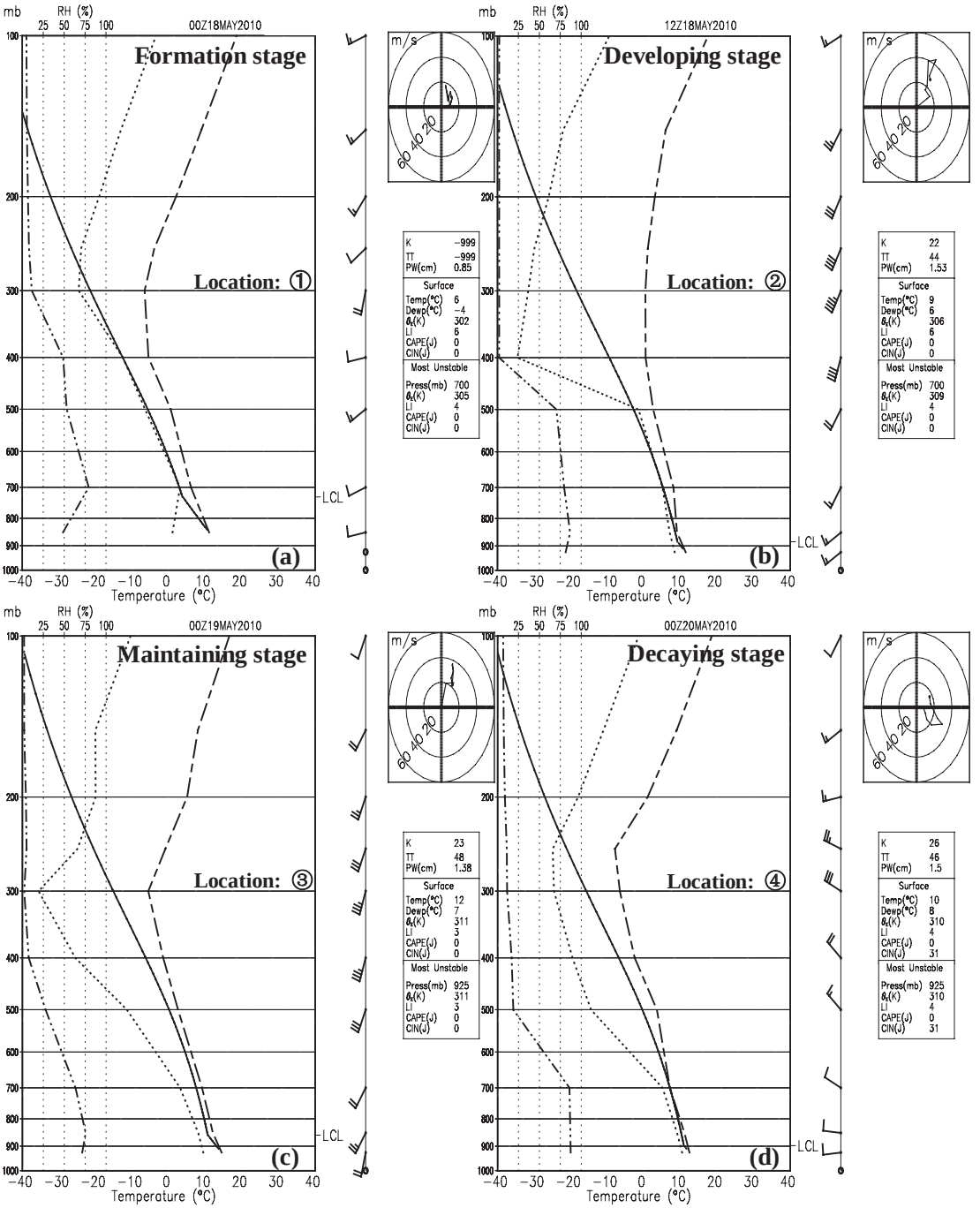

Fig. 7. Observed typical soundings at different stages (①–④ in Fig. 5) of the NCCV, where dashed-dotted lines are relative humidity (RH), dotted lines are dew point, dashed lines are temperature, solid lines are air-mass-lifting lines, and LCL stands for the lifting condensation level.

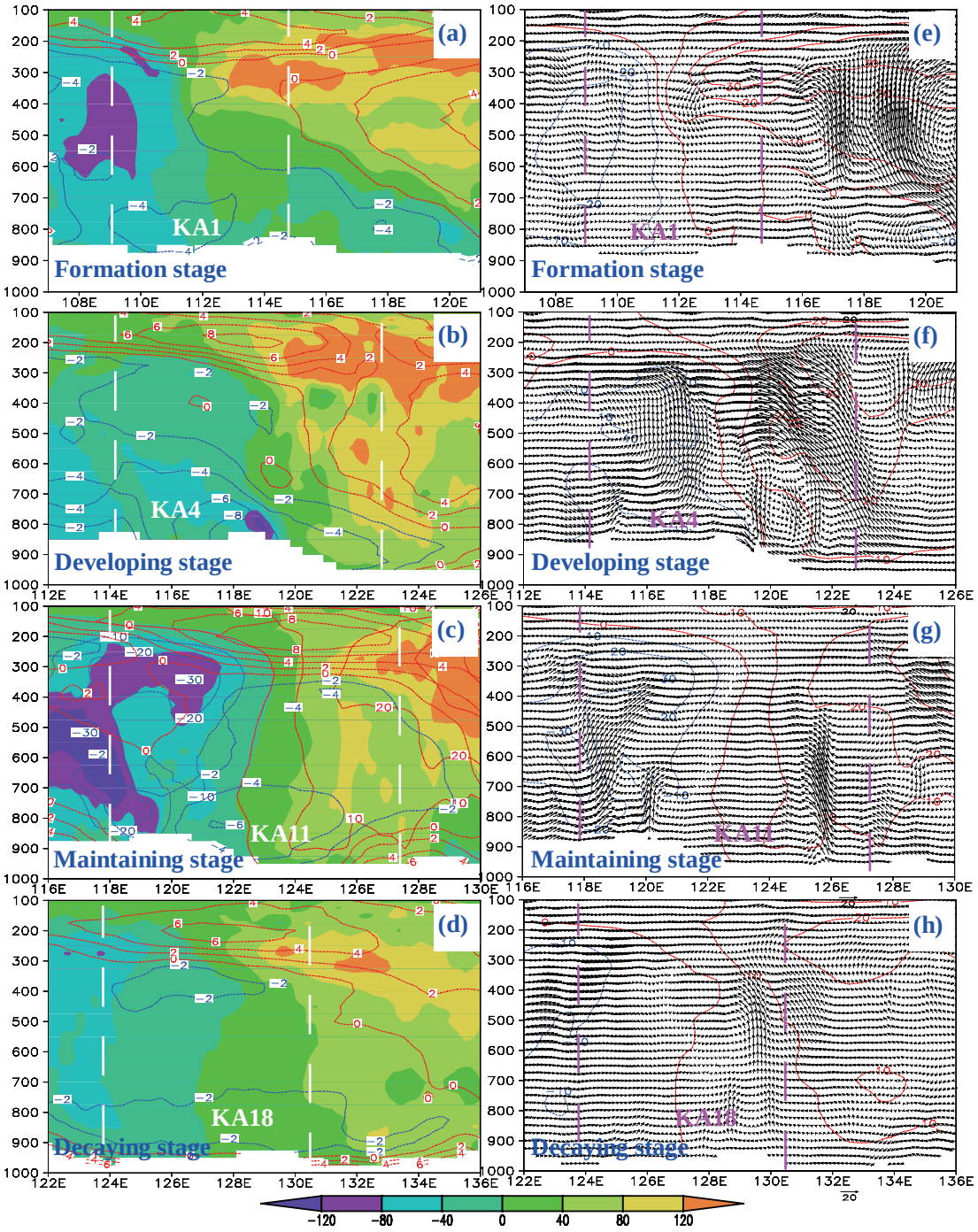

Fig. 8. Cross sections along the central latitudes of the NCCV at typical stages, where the left column depicts the horizontal temperature advection (shaded, units: 10^{-5} K s^{-1}) and the temperature deviation (the red and blue dashed lines, units: °C); and the right column represents the meridional velocity (the blue and red solid lines, units: m s^{-1}) and the composed vector of zonal wind and vertical velocity × 100 (units: m s^{-1}). The thick white and purple dashed lines represent the KAs of the NCCV. (a) and (e) are at 0000 UTC 18 May; (b) and (f) are at 0900 UTC 18 May; (c) and (g) are at 0600 UTC 19 May; and (d) and (h) are at 0300 UTC 20 May.

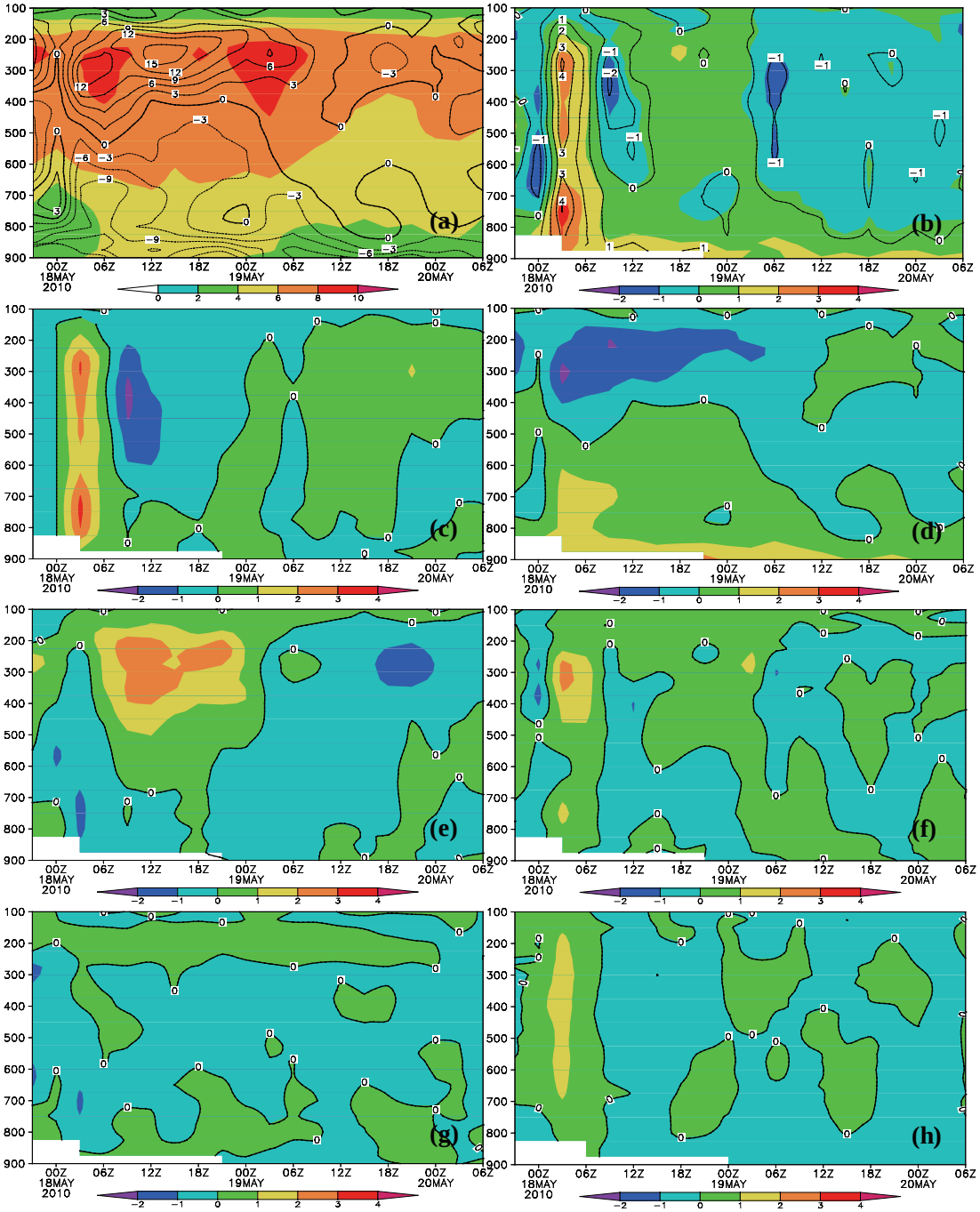

Fig. 9. Cross sections of KA-averaged vorticity, divergence, and results of the EFC budget equation, where panel (a) depicts the averaged vorticity (shaded, units: 10^{-5} s^{-1}) and divergence (contour, units: 10^{-6} s^{-1}); (b) the total effect of the right-hand side terms of the EFC budget equation except for the RES term (solid) and KA-averaged Lagrangian variation (shaded); (c) motion-caused flux; (d) stretching; (e) background flux; (f) eddy flux; (g) tilting; and (h) RES. The solid line in figures c–h is the value of 0, and all averaged terms of the EFC budget equation have the same units: 10^{-9} s^{-2}.

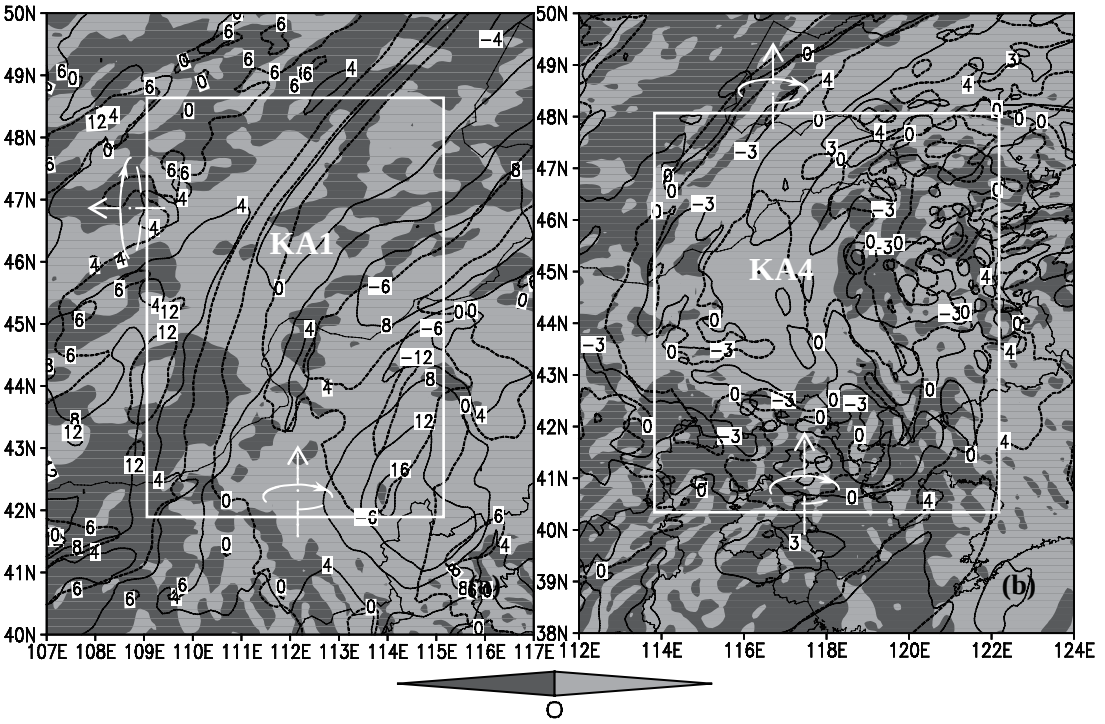

Fig. 10. The vertical motion (dark gray represents downdraft, light gray stands for updraft), the vertical shear of zonal wind (solid, unit: m s^{-1}), and the vertical shear of meridional wind (dashed, unit: m s^{-1}), where vectors stand for the angular velocity vector norm to the boundary line, and the ellipses represent the circulation around the angular velocity vector. (a) 1800 UTC 17 May at 300 hPa, and (b) 0900UTC 18 May at 500 hPa.

eddy flux, detailed analyses were employed at typical stages. In the motion-caused flux term ($\overrightarrow{M}_h \cdot \nabla_h C$), when the angle between $\overrightarrow{M}_h$ and $\nabla_h C$ is less than 90º, namely, as the system moves from areas of low circulation (low vorticity) to areas of high circulation (high vorticity)[4], the motion-caused flux is favorable for enhancing cyclonic circulation. The NCCV moved northeastward, and Fig. 11a shows that the NCCV generally moved from low-vorticity zones to higher-vorticity zones. Therefore, the displacement was favorable for the development of the NCCV, and at 0300 UTC 18 May, a positive center of the motion-caused flux appeared at approximately 300 hPa (Fig. 9c).

At 0600 UTC 18 May, a positive center of eddy flux appeared at approximately 300 hPa (Fig. 9f), which was conducive to the development of the NCCV. The wind perturbation transported the positive vorticity perturbation into KA3 and transported negative vorticity perturbation out across the western boundary, conditions that were very favorable for the enhancement of the cyclonic circulation of the NCCV (Fig. 12a). Similarly, the wind perturbations around the northern, southern, and eastern boundaries of KA3 were all generally favorable for the enhancement of the cyclonic circulation of the NCCV. The eddy flux became negative at approximately 500 hPa at 1200 UTC 18 May (Fig. 9f). Generally, the wind perturbation transported the negative vorticity perturbation into KA5 (Fig. 12b), which acted to weaken the cyclonic circulation of the NCCV; therefore, the eddy flux was detrimental to the NCCV.

Compared with the other terms, the tilting term was weak; however, a positive area appeared at approximately 500 hPa at 0900 UTC 18 May (Fig. 9g) that was conducive to the development of the NCCV. The vertical shear of the zonal wind was mainly positive at the northern and southern boundaries of KA4 (Fig.

[4]There is a relationship between the circulation and vorticity, namely, $C = \oint_l \vec{V} \cdot d\vec{l} = \iint_A (\nabla \times \vec{V}) \cdot d\vec{A}$, where C is circulation, l the boundary line of area A. As a result, vorticity could be regard as a measure of circulation.

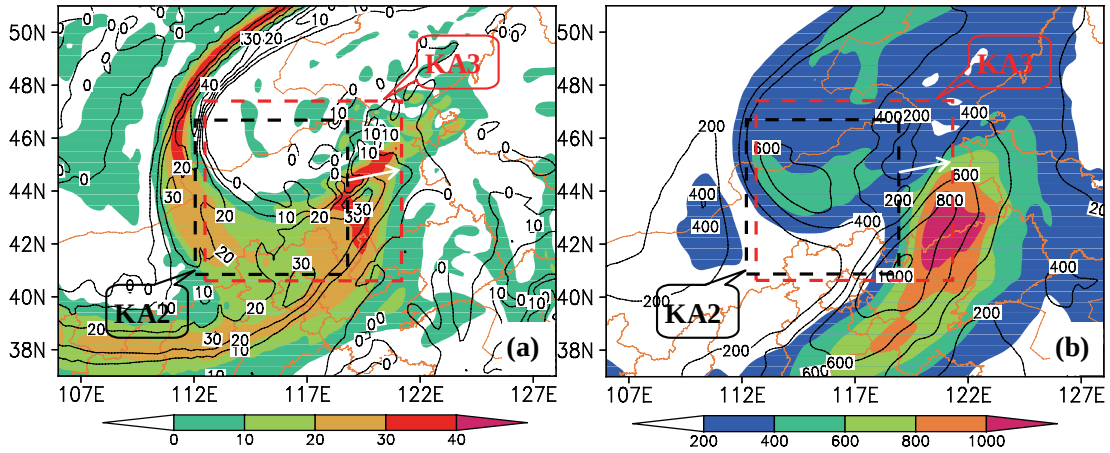

Fig. 11. The distribution of vorticity (unit: 10^{-5} s^{-1}) and EKE (unit: J kg^{-1}) at 300 hPa, where the black and red dashed rectangles are key areas of the NCCV. The solid in (a) is the vorticity distribution at 0300 UTC 18 May, while the shaded is the vorticity distribution at 0600 UTC 18 May; and the solid in (b) is the EKE distribution at 0300 UTC 18 May, while the shaded is the EKE distribution at 0600 UTC 18 May.

10b); thus, the angular velocity vectors both pointed to the north. Because the ascending motions dominated the northern boundary of KA4, the lifting of the angular velocity vector enhanced the easterly wind along the northern boundary, favoring the intensification of the cyclonic circulation of the NCCV. The descending motions dominated the southern boundary of KA4 (Fig. 10b), which enhanced the westerly wind along the boundary, thus enhancing the cyclonic circulation of the NCCV.

c. The Maintaining stage (1800 UTC 18 May to 1800 UTC 19 May)

The convergence in the middle-lower troposphere and the divergence in the upper troposphere both weakened significantly (Fig. 9a). Moreover, convergence appeared in the upper troposphere during the later period of the maintaining stage (Fig. 9d). The total effects (Fig. 9b) mainly remained positive during the initial period of the maintaining stage, whereas the effects changed to negative during the later stage, indicating that the NCCV had begun to weaken. The displacement was mainly favorable for sustaining the NCCV (Fig. 9c), and the stretching term due to convergence dominated the EFC budget in the LLN (Fig. 9d).

During the initial period of the maintaining stage, the transport by the background circulation was favorable for the maintenance of the NCCV in the ULN, whereas this transport acted conversely in the LLN (Fig. 9e). During the later period of the maintaining stage, the background flux was mainly detrimental to the NCCV. The eddy flux term was mainly favorable for the sustainment of the vortex, although it changed to a negative value in the ULN during the latter period of the maintaining stage (Fig. 9f). The tilting term was mainly detrimental to sustaining the NCCV (Fig. 9g).

d. The decaying stage (1800 UTC 19 May to 0600 UTC 20 May)

The convergence remained in the lower and upper troposphere (Fig. 9a), with weak divergence maintained in the mid-troposphere; thus, the stretching term was favorable for the sustainment of the vortex at the lower and upper troposphere (Fig. 9d), whereas this term was detrimental to the maintenance of the NCCV in the mid-troposphere. The displacement of the NCCV was very favorable for sustaining the vortex at the ULN, whereas it was detrimental to the NCCV at the LLN (Fig. 9c). The transport by the background circulation accelerated the decay of the NCCV in the ULN remarkably (Fig. 9e) but acted conversely in the LLN. The eddy flux term was mainly favorable for the sustainment of the NCCV in the ULN (Fig. 9f), whereas in the LLN, it was first detrimental to the NCCV and then acted conversely. The tilting term was mainly detrimental to the maintenance of the vortex in the levels from 700–250 hPa (Fig. 9g), whereas this term acted oppositely below 700 hPa.

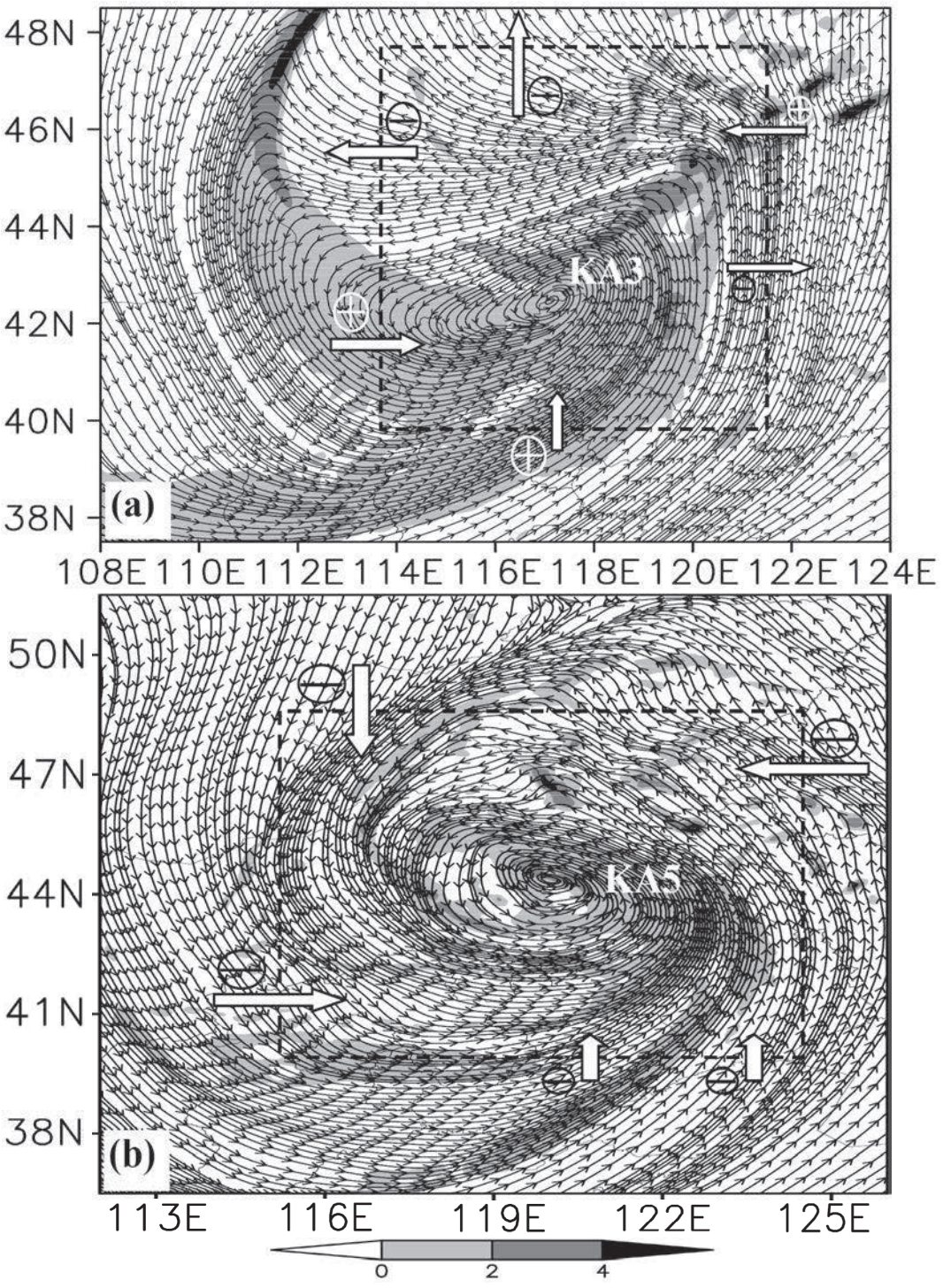

Fig. 12. The eddy flux of vorticity perturbation at different levels, where the shaded is the vorticity perturbation (10^{-4} s^{-1}), the solid is the stream field of the wind perturbation, dashed rectangles are key areas of the NCCV, arrows are the main direction of the wind perturbation, and the negative and positive sign with a circle stand for the sign of the vorticity perturbation. (a) is 0600 UTC 18 May at 300 hPa, and (b) is 1200 UTC 18 May at 500 hPa.

4.2. The EKE budget results

An intense zone of EKE remained at approximately 300 hPa, corresponding to the NCCV with the maximum center appearing during the initial period of the maintaining stage (Fig. 13a), and the EKE weakened significantly during the latter period of the maintaining stage, corresponding to the decaying of the vortex. The ascending motions remained very intense during the developing stage and then weakened during the maintaining stage; descending motions occurred during the decaying stage (Fig. 13a). Compared with that shown in Fig. 9a, the variation of the EKE was approximately consistent with that of the vorticity during the formation, developing and maintaining stages; while during the decaying stage, the EKE dissipated earlier than the vorticity (Figs. 13a, 9a), which indicates that the decaying process of the NCCV may be closely related to the frequency dispersion of the baroclinic Rossby wave. The overall, well balanced EKE budget revealed that neglecting the *RES* term was not detrimental to obtaining a nearly balanced budget (Figs. 13b, c); therefore, the EKE budget results can be used for further research.

During the formation stage, the baroclinic and barotropic energy conversions were mainly favorable for the enhancement of the EKE in the LLN but detrimental to the EKE in the ULN (Figs. 13d, e). The horizontal transport by background circulation (Term 3) was conducive to the enhancement of the EKE in the LLN but detrimental to the EKE in the ULN (Fig. 13f), and the vertical transport by background circulation (Term 4) was conducive to the enhancement of the EKE in the ULN but detrimental to the EKE in the LLN (Fig. 13g). The horizontal and vertical transport of geopotential perturbations by the synoptic perturbations dominated the EKE budgets in the LLN and ULN, respectively (Figs. 13i, j)

During the developing stage, the EKE of the NCCV increased with time and stretched downward (Fig. 13a), in good agreement with the development of the vortex (Fig. 6). The barotropic and baroclinic energy conversions both enhanced significantly, providing very favorable conditions for the development of the NCCV (Figs. 13d, e). The horizontal transport of EKE by background circulation was conducive to the enhancement of the EKE in the LLN but detrimental to the EKE in the ULN (Fig. 13f); and the vertical transport of EKE by background circulation was conducive to the enhancement of the EKE in the ULN but detrimental to the EKE in the LLN (Fig. 13g). As discussed in Sub-subsection 4.1.b, the expression of Term 5 in Eq. (3) indicates that the EKE of the system increases as it moves from areas of low to high EKE. As shown in Fig. 13h, the displacement was favorable for an increase of EKE, and Fig. 11b shows that the NCCV generally moved from low-EKE areas to higher-EKE areas; therefore, the displacement was conducive to the enhancement of the EKE. The horizontal and vertical transport of geopotential perturbations by synoptic perturbations were very favorable for the increase of the EKE in the ULN and LLN, respectively (Figs. 13i, j). However, the horizontal and vertical transport of geopotential perturbations by synoptic perturbations served as EKE sinks in the LLN and the ULN, respectively.

The EKE associated with the NCCV remained intense during the initial period of the maintaining stage and then decreased during the latter period of the maintaining stage (Fig. 13a). The barotropic and baroclinic energy conversions both weakened (Figs. 13d, e), and the barotropic energy transition changed to a negative value during the latter period of maintaining stage. The horizontal transport of EKE by background circulation was mainly detrimental to the EKE (Fig. 13f), whereas the vertical transport by background circulation was still conducive to the EKE in the ULN (Fig. 13g). The displacement of the NCCV and the horizontal transport of geopotential perturbations by synoptic perturbations (Term 6) were favorable for sustaining the EKE in the ULN, but both were detrimental to the EKE in the LLN (Figs. 13h, i). The vertical transport of geopotential perturbations by synoptic perturbations (Term 7) dominated the maintenance of EKE in the LLN, whereas this term mainly acted conversely in the ULN (Fig. 13j).

During the decaying stage, the EKE weakened significantly (Fig. 13a). The barotropic and baroclinic energy conversions were both mainly detrimental to the sustainment of EKE during the initial period of this stage (Figs. 13d, e), whereas these conversions were mainly favorable for the maintenance of the EKE during the latter period. The vertical transport of EKE by background circulations, the displacement and the horizontal transport of geopotential perturbations by synoptic perturbations were all conducive to sustaining the EKE in the ULN (Figs. 13g–i), whereas the horizontal transport of EKE by background circulation and the vertical transport of geopotential perturbations by synoptic perturbations were favorable for the maintenance of the EKE in the LLN (Figs. 13f–j). The horizontal transport of EKE by background circulations and the vertical transport of geopotential perturbations by synoptic perturbations dominated the decay of EKE in the ULN, whereas the horizontal transport of geo-

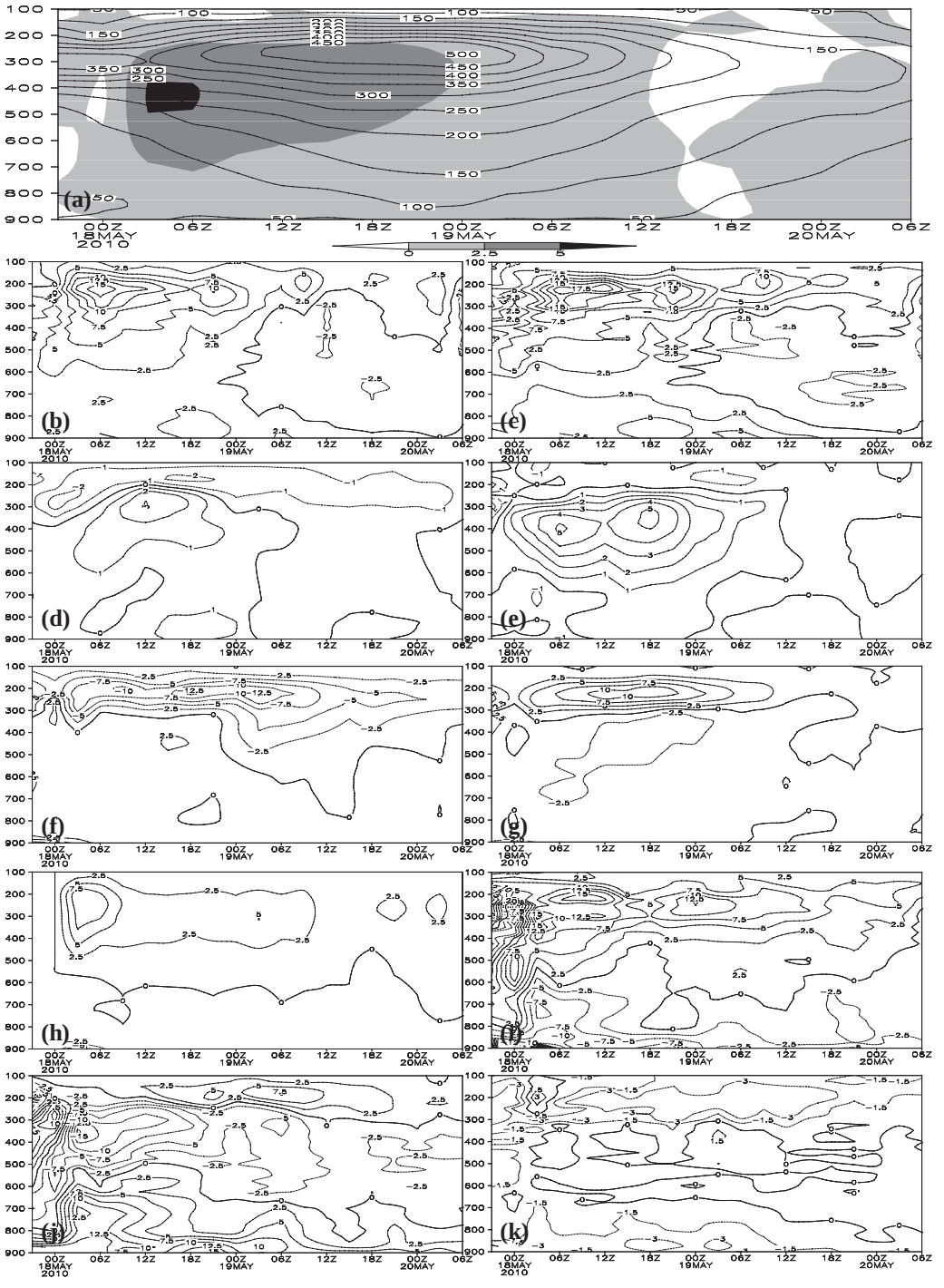

Fig. 13. Cross sections of KA-averaged EKE and results of EKE budget equation. (a) the KA-averaged EKE (solid, unit: J kg^{-1} m^{-2}) and vertical motions (shaded, unit: m s^{-1}); (b) Lagrangian variation of the NCCV; (c) term total; (d) barotropic energy transition; (e) baroclinic energy transition; (f) horizontal flux divergence of EKE by background circulations; (g) vertical flux divergence of the EKE by background circulations; (h) horizontal divergence of EKE caused by system motion; (i) horizontal eddy flux divergence of eddy geopotential energy; (j) vertical eddy flux divergence of eddy geopotential energy; (k) RES;. The units of panels b–k are 10^{-3} J kg^{-1} m^{-2} s^{-1}.

Table 1. The factors dominating the intensification of cyclonic circulation and EKE during the formation, developing and maintaining stages, and the factors dominating the weakening of cyclonic circulation and EKE during the decaying stage of the NCCV.

Layers and methodology		The formation stage	The developing stage		The maintaining stage		The decaying stage
			Initial period	*Later period*	*Initial period*	*Later period*	
Upper levels of the NCCV	EFC	Background Flux	Motion-caused Flux Eddy Flux	Background Flux	Background Flux Eddy Flux	Motion-caused Flux	Background Flux
	EKE	Term 7	Term 4 Term 5 Term 6	Term 2 Term 6	Term 2 Term 5 Term 6	Term 6	Term 3 Term 7
Lower levels of the NCCV	EFC	Stretching	Stretching Motion-caused Flux	Stretching	Stretching	Stretching Eddy Flux	Motion-caused Flux RES
	EKE	Term 6	Term 7	Term 7	Term 7	Term 7	Term 4 Term 6

potential perturbations by synoptic perturbations (Fig. 13i) and the vertical transport of EKE by background circulations (Fig. 13g) dominated the decrease of the EKE in the LLN.

5. Summary and conclusions

In this study, a typical NCCV with several heavy rainfall events during the spring of 2010 was investigated to enhance our understanding of the NCCV including its structure, evolution, and interactions with other systems. Moreover, a more detailed explanation of the tilting term was formulated from a circulation viewpoint, and the results agreed well with the work of Davis and Galarneau (2009).

The NCCV is a deeply developed vortex with maximum vertical stretching from 900 hPa to 200 hPa in the present case. The NCCV was very intense in the middle-upper troposphere, and there were obvious 200-hPa ULJ and 700-hPa LLJ associated with the vortex. The LLJ transported moisture from the Bohai Sea, the Yellow Sea, and the Sea of Japan to the NCCV area, which was favorable for precipitation. The NCCV was colder than its surroundings below 300 hPa, which is the reason for the name "cold vortex", whereas warm areas remained above 300 hPa. During the entire lifetime of the NCCV, there were significant cold and warm advections. The intense intersection of warm and cold air favored the enhancement of APE which was in turn conducive to the maintenance of the NCCV.

The NCCV displayed a very complicated evolution. The EFC and EKE budget equations were employed to analyze the evolution mechanisms of the NCCV, and the terms that dominated the evolution of the vortex are summarized in Table 1. Generally, for the EFC budget, the interactions between the vortex and background circulations were more important than the interactions between the NCCV and other synoptic systems. However, for the EKE budget, the interactions between the NCCV and other synoptic perturbations were more important. Therefore, the interactions with other synoptic systems were more important in determining the intensity of the NCCV, whereas the interactions with the background circulations were more important in determining the flow pattern of the NCCV.[5] The displacement of the NCCV was important to the evolution of the vortex, especially during the developing and maintaining stage; the circulation (EKE) increased when the NCCV moved from low- to high-vorticity (EKE) areas, which indicates that the pattern of vorticity distribution (i.e., the characteristics of the environmental circulations) and EKE (i.e., the distribution of synoptic perturbations) were very important for the development of the NCCV.

For the duration of the NCCV, the wind shear between 300 and 700 hPa remained significant, which indicates that the baroclinity of the NCCV was very strong. Moreover, the results of the EKE budget show

[5]The EKE is closely related to the intensity of the synoptic system, whereas the circulation reflects only the flow pattern of a synoptic system (such as cyclonic or anticyclonic) and is closely related to the redistribution of EKE.

that the baroclinic energy conversion, which is closely related to the release of APE, was much greater than the barotropic energy conversion; thus, the NCCV is a typical baroclinic cyclone. The variation of positive vorticity was consistent with that of the EKE (Figs. 9a, 13a) approximately during the formation, developing and maintaining stages; whereas during the decaying stage, the EKE dissipated earlier than the positive vorticity, which may have been caused by the frequency dispersion processes of the baroclinic Rossby wave.

Although a typical NCCV in the spring of 2010 was thoroughly studied in this work, other cases should be analyzed in the future to obtain a more complete understanding of this type of vortex. A composite analysis of NCCVs will be performed in a following study, providing an efficient means for better understanding the formation and evolution of NCCVs.

Acknowledgements

This research was supported by the National Natural Science Foundation of China (Grant Nos. 41075032 and 40930951) and the National Key Basic Research and Development Project (Grant No. 2012CB417201). We thank the NCAR for providing the final analysis data, and we sincerely thank the editor and the reviewers for their very valuable advice.

References

Bai, R.-H., 1997: The intensive observational fact analysis on cold vortex over Northeast China. *Heilongjiang Meteorology*, **4,** 1–3.

Davis, C. A., and T. J. Galarneau, 2009: The vertical structure of mesoscale convective vortices. *J. Atmos. Sci.,* **66,** 686–704.

Ding, Y.- H., and Y.-Z. Liu, 1985: On the analysis of Typhoon kinetic energy -I- budget 0f total kinetic energy and EKE. *Science in China Series B,* **15**, 957–966.

Fu, S.-M., J.-H. Sun, S.-X. Zhao, and W.-L. Li, 2009: An analysis of the EKE budget of a southwest vortex during heavy rainfall over south China. *Atmos. Oceanic Sci. Lett.,* **2,** 135–141.

He, J.-H., Z.-W. Wu, Z.-H. Jiang, C.-S. Miao, *et al*., 2006: "climate effect" of the northeast cold vortex and its influences on Meiyu. *Chinese Science Bulletin,* **51,** 2803–2809.

Hong, S.-Y., Y. Noh, and J. Dudhia, 2006: A new vertical diffusion package with an explicit treatment of entrainment processes. *Mon. Wea. Rev.*, **134**: 2318–2341.

Huang, X.-J., Q.-W. Zhu, and S. Liu, 1997: *The characteristic analyses on East Asia block in the activity period of cold vortex over Northeast China in early summer*. Liaoning Publishing House, 30–34.

Kain, J. S., and J. M. Fritsch, 1990: A one-dimensional entraining/detraining plume model and its application in convective parameterization. *J. Atmos. Sci.*, **47**, 2784–2802.

Kain, J. S., 2004: The Kain-Fritsch convective parameterization: an update. *J. Appl. Meteor.,* **43**, 170–181

Liu, S.-C., and B.-Q. Liang, 1993: The perturbation - kinetic energy budget of the monsoon depressions over the south China sea. *Tropic Oceanology,* **12**, 1–8.

Liu, Z.-X., Y. Lian, Z.-T. Gao, L. Sun, *et al.*, 2002 : Analyses of the northern Hemisphere circulation characters during northeast cold vortex persistence. *Chinese Journal of Atmospheric Sciences,* **26,** 361–372.

Mao, X.-M., and X.-B. Qv, 1997: Energetics analysis of a cold vortex in Northeast China. Acta Meteorologica Sinica, **55**, 230–238.

Michalakes, J., J. Dudhia, D. Gill, T. Henderson, J. Klemp, W. Skamarock, and W. Wang, 2004: The Weather Reseach and Forecast Model: Software Architecture and Performance, to appear in proceedings of the 11th ECMWF Workshop on the Use of High Performance Computing In Meteorology, 25–29 October.

Orlanski, I., and J. Katzfey., 1991: The life cycle of a cyclone wave in the Southern Hemisphere Part I. Eddy energy budget. *J. Atmos. Sci.,* **48**, 1972–1998.

Palmen, E., and C. W. Newton, 1969: *Atmospheric circulation systems*. Academic Press, 603 pp.

Price, J. D., and G. Vaughan, 1992: Statistical studies of cut-off low systems. *Ann Geophys.,* **10**, 96–102.

Qi, Y.-B., X.-L. Guo, and D.-Z. Jin, 2007: An observational study of macro/microphysical structures of convective rainbands of a cold vortex over northeast China. *Chinese Journal of Atmospheric Sciences,* **31,** 621–634.

Qiao, F.-X., S.-X. Zhao, and J.-H. Sun, 2007: Study of the vorticity and moisture budget of a northeast vortex producing heavy rainfall. *Climatic and Environmental Research,* **12,** 397–412.

Shou, Y.-X., and J.-M. Xu, 2007: The rainstorm and mesoscale convective systems over northeast China in June 2005. II: A synthetic analysis of MCS's dynamical structure by radar and satellite observations. *Acta Meteorologica Sinica,* **65,** 171–182.

Sun, L., X.-Y. Zheng, and Q. Wang, 1994: The climatological characteristics of northeast cold vortex China. *Acta Meteorologica Sinica,* **5,** 297–303.

Sun, L., G. An, Y. Lian *et al.*, 2000: A study of the persistent activity of northeast cold vortex in summer and its general circulation anomaly characteristics. *Acta Meteorologica Sinica,* **55,** 704–714.

Tao, S.-Y., 1980: *Rainstorms in China*. Scientific Press, 225pp.

Trigo, I., T. D. Davies, and G. R. Bigg, 1999: Objective climatology of cyclones in the Mediterranean region. *J. Climate,* **12**, 1685–1696.

Wang, D.-H., S.-X. Zhong, Y. Liu, J. Li, *et al.*, 2007: Advances in the study of rain storm in northeast China. *Advances in Earth Science,* **22,** 549–560.

Zhang, Y., H.-C. Lei, and Z.-C. Qian, 2008: Analyses of for-

mation mechanisms of a rainstorm during the declining phase of a northeast cold vortex. *Chinese Journal of Atmospheric Sciences,* **32,** 481–498.

Zhang, L.-X., and Z.-C. Li. 2009: A summary of research on cold vortex over Northeast China. *Climatic and Environmental Research,* **14,** 218–228.

Zhao, S.-X., S.- H. Liu, and M.-Y. Liu, 1980: Mesoscale analysis of strong convective weather system caused by cold vortex over Beijing during summer. In *Collected Papers of Institute of Atmospheric Physics, Chinese Academy of Sciences, No.9*. Institute of Atmospheric Physics, Chinese Academy of Sciences, 151–160.

Zhao, S.-X., and J.-H. Sun, 2007: Study on Cut-off Low-Pressure Systems With Floods over Northeast Asia. *Meteorol. Atmos. Phys.,* **96**, 159–180.

Zheng, X.-Y., T.-Z. Zhang, and R.-H. Bai, 1992: *Rainstorm in Northeast China*. Metrorological Press, 219 pp.

Zhou, L., 1991: *Climate in Northeast China*. China Meteorological Press, 122 pp.

Zhu, Q.-W.,1997: The study on circulation evolvement characteristic of cold vortex over Northeast China and relation among weather systems. In *Corpus of Research on Cold Vortex over Northeast China*. Liaoning Publishing House, 14–29.